

Multomics Analysis Unravels Alteration in Molecule and Pathways Involved in Nondiabetic Chronic Wounds

Shuaidan Zeng, Zijun Zheng, Xuerong Wei, Lianglong Chen, Jiabao Lin, Mengqian Liu, Kaize Zheng, Weiqing Li, Xiaodi Chen, Jun Ma, Zhu Xiong,* and Lei Yang*



Cite This: *ACS Omega* 2024, 9, 20425–20436



Read Online

ACCESS |

Metrics & More

Article Recommendations

Supporting Information

ABSTRACT: The prevalence of chronic wounds (CW) continues to grow. A thorough knowledge of the mechanism of CW formation remains elusive due to a lack of relevant studies. Furthermore, most previous studies concentrated on diabetic ulcers with relatively few investigations on other types. We performed this multiomics study to investigate the proteomic and metabolomic changes in wound and surrounding tissue from a cohort containing 13 patients with nondiabetic CW. Differentially expressed proteins (DEPs) and metabolites (DEMs) were filtered out and analyzed through multiomic profiling. The DEPs were further confirmed with the use of parallel reaction monitoring. Compared with the surrounding tissue, there were 82 proteins and 214 metabolites altered significantly in wound tissue. The DEPs were mainly enriched in focal adhesion (FA), extracellular matrix–receptor interaction (ERI), and the PI3K–Akt (PA) signaling pathway. Moreover, the DEMs were significantly enriched in amino sugar and nucleotide sugar metabolism and biosynthesis of nucleotide sugar pathways. In correlation analysis, we discovered that the PA signaling pathway, as well as its upstream and downstream pathways, coenriched some DEPs and DEMs. Additionally, we found that FBLN1, FBLN5, and EFEMP1 (FBLN3) proteins dramatically elevated in wound tissue and connected with the above signaling pathways. This multiomics study found that changes in FA, ERI, and PA signaling pathways had an impact on the cellular activities and functions of wound tissue cells. Additionally, increased expression of those proteins in wound tissue may inhibit vascular and skin cell proliferation and degrade the extracellular matrix, which may be one of the causes of CW formation.



1. INTRODUCTION

Repairing chronic wounds (CWs) has proven challenging, and the condition has been highlighted as a potential pandemic disease globally. CW has a major detrimental influence on patients' capacity to work and live normally and imposes an enormous burden on families and society.^{1,2}

The CW refers to the wound caused by various factors that cannot completely heal within an expected time according to biological law after conventional treatment intervention. The duration of wounds ranged from 4 weeks to 3 months.³

Diabetic ulcers (DU) are the focus of a majority of current CW research. Many factors affecting wound healing in diabetic patients have been investigated through a series of omics studies: hypoxic wound environment, toxic effects of necrotic cells, excessive activation of neutrophils and macrophages, and excessive ROS secretion in a high glucose environment, leading to extracellular matrix (ECM) degradation and growth factor degeneration. Altered cell function and mobility result in neovascularization and tissue development. Moreover, keratinocyte and fibroblast migration and proliferation are inhibited, while apoptosis is enhanced, leading to epidermal formation abnormalities.^{4–11}

However, there are few studies on other types of CW. For instance, pressure ulcers (PUs) and traumatic ulcers (TUs), both of which can form at any age, can even cause morbidity in children. Their pathogenesis, clinical manifestations, and treatment methods are also different from those of DU. The main pathophysiological triggers of DU include neuropathy, infection secondary to trauma, and arterial occlusive disease. Atherosclerosis is also an important cause.^{12,13}

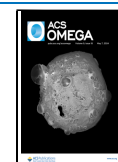
PU is usually caused by pressure, and its essence is long-term ischemia–reperfusion injury. When the blood supply of the tissue is exhausted, its metabolism will be reduced to maintain its function, and reperfusion will produce excessive oxygen free radicals, causing cytotoxic effects.¹⁴ Hence, research on other types of CW might aid clinical diagnosis and guide treatment

Received: February 10, 2024

Revised: April 8, 2024

Accepted: April 12, 2024

Published: April 25, 2024



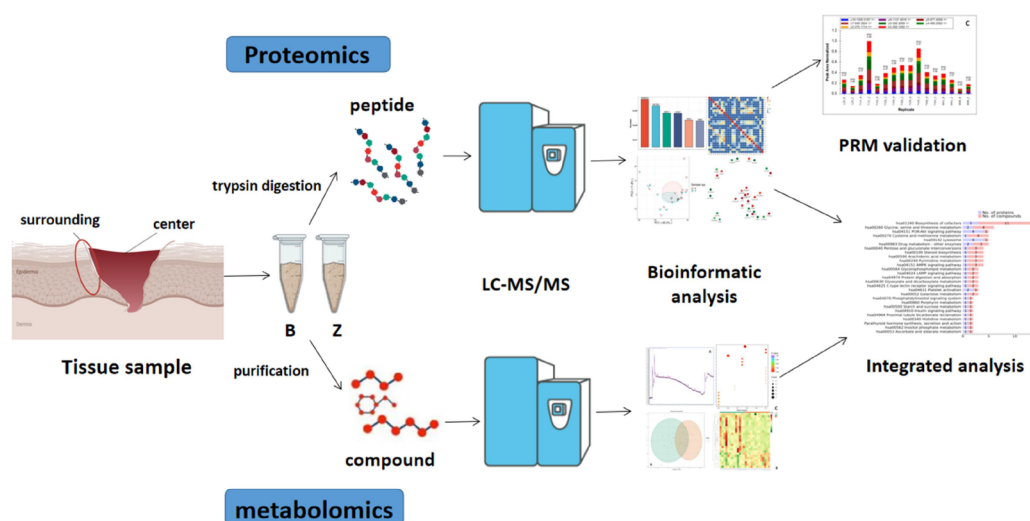


Figure 1. Schematic diagram of proteomics, metabolomics, and integrated analysis procedure of tissue samples.

as well as provide a more comprehensive knowledge of the molecular processes causing CW.

Large-scale, cost-effective multiomics analyses are starting to be employed more often as a result of advancements in next-generation sequencing technology and high-resolution MS.^{15,16} Future advances in precision medicine and translational medicine will greatly benefit from the analysis of biological samples at multiple omics levels because it may assist in the formation of disease models, prognostic prediction, and investigation into how effectively disorders react to therapy and a better understanding of how diseases arise and progress. The development of CW is a complex process involving several components, such as cytokines, proteins, metabolites, and signaling pathways. Proteomics combined with metabolomics analysis can provide a more thorough understanding of the CW microenvironment.

Thus, to investigate the molecular mechanisms and associated signaling pathways, as well as to identify candidate biomarkers and potential therapeutic targets, this research explored the changes in the proteome and metabolome of the wound and surrounding healed tissues in patients with CW.

2. MATERIAL AND METHODS

A graphical representation regarding the sample collection as well as the workflow of multiomics analysis is shown in Figure 1.

2.1. Study Population. Patients who met the criteria for diagnosis of CWs between January 2022 and December 2022 were included in the present research. However, patients with diabetes, hypertension, arthrolithiasis, malignancy, heart/liver, and other important organ diseases, immune/metabolic diseases, regular medication intake, or previous surgery were excluded.

The study protocol received approval from the Nanfang Hospital Ethics Committee of Southern Medical University, since it accorded with the ethical guidelines stated in the Declaration of Helsinki. Every patient or guardian provided their informed consent.

2.2. Collection of Wound Tissue. We excised all of the wound tissue and a portion of the wound edge tissue (which had healed but stopped healing), in accordance with the standard CW surgery procedure. For further investigation and

comparison, the wound's center tissue (group Z) and surrounding tissue (group B) were removed individually. The sampling will not cause extra injury to the patients. After the excised tissues were rinsed in double-distilled water, they were placed immediately in sterile cryovials and preserved in a $-80\text{ }^{\circ}\text{C}$ refrigerator.

2.3. Proteomics Analysis. **2.3.1. Sample Preparation.** The samples were placed in a 5-mL centrifuge tube after being ground into a powder under liquid nitrogen. Four volumes of lysis solution (8 M urea, 1% protease inhibitor combination) were added to the powder and sonicated three times on ice using a Scientech high-intensity ultrasonic processor. The lysis buffer was enhanced by the addition of inhibitors. To remove the remaining fragments, centrifugation was applied for 10 min at $4\text{ }^{\circ}\text{C}$ and 12,000g. Finally, the protein content was identified by collecting the supernatant in the BCA kit.

For support in digestion, the protein solution was reduced for 30 min at $56\text{ }^{\circ}\text{C}$ using 5 mM dithiothreitol and alkylated for 15 min at room temperature in the dark using 11 mM iodoacetamide. Subsequently, a urea concentration of less than 2 M was mixed with 100 mM TEAB to dilute the protein sample. Finally, trypsin was introduced at a ratio of 1:100 for the first digestion of the protein mass overnight and 1:50 for the second digestion that took place over 4 h. Ultimately, the peptides were desalted using a C18 SPE column.

2.3.2. LC-MS/MS Analysis. The tryptic peptides were diluted in solvent A (0.1% formic acid, 2% acetonitrile/in water) and then separated using the Bruker Daltonics nanoElute UHPLC system. Peptides were separated using a gradient that progressed from 6 to 24% solvent B (0.1% formic acid in acetonitrile) over 70 min, 24 to 35% in 14 min, rising to 80% in 3 min, and holding at 80% for the last 3 min. The gradient was applied at a constant flow rate of 450 nL/min.

Following their exposure to a capillary source, the peptides were subjected to mass spectrometry applying Bruker Daltonics' timsTOF Pro 2. The electrospray voltage employed was 1.60 kV. Precursors and fragments were analyzed using the TOF detector with an MS/MS scan range of 100 to 1700 m/z . Data are collected using the Parallel Accumulation-Serial Fragmentation (PASEF) method. Precursors with charge states between 0 and 5 were chosen for fragmentation based on 10

PASEF-MS/MS images collected each cycle. The dynamic exclusion of the 1930s was used.

2.3.3. Database Search. To process the generated MS/MS data, the MaxQuant search engine (v.1.6.15.0) was applied. Homo_sapiens_9606_SP_20220107.fasta (20,376 sequences) was the search database chosen. Trypsin/P was specified as a cleavage enzyme, allowing up to two missing cleavages. The mass error tolerance for precursor ions was 20 ppm for the first search and 4.5 ppm for the main search. The mass error tolerance for fragment ions was established at 20 ppm. Variable modifications were identified as acetylation on the protein's N-terminus and oxidation on Met, whereas fixed changes were identified as carbamidomethyl on Cys. The false positive rate for protein and PSM identification was 1% (FDR).

2.3.4. Bioinformatics Methods. The UniProt-GOA database (<https://www.ebi.ac.uk/GOA/>) provided the Gene Ontology (GO) annotation for the proteome. InterProScan, an application that assesses data using protein sequence alignment and the InterPro domain database (<https://www.ebi.ac.uk/interpro/>), was used to annotate the functional descriptions of protein domains discovered in this investigation. The Kyoto Encyclopedia of Genes and Genomes (KEGG) database (<https://www.kegg.jp/kegg/pathway.html>) was utilized to determine enriched pathways, and the degree of protein enrichment in relation to all identified proteins was evaluated using a two-tailed Fisher's exact test. Routes with a corrected P-value of less than 0.05 were classified as significant and kept apart. The STRING database (v11.0) was thoroughly analyzed in order to visualize every differentially expressed protein (DEP) accession number or sequence within the protein–protein interaction (PPI) network.

2.3.5. Parallel Reaction Monitoring Validation. Based on sequencing results, the proteins were selected for validation through parallel reaction monitoring (PRM). Liquid chromatography solvent A (0.1% formic acid and 2% acetonitrile) was utilized to dissolve the tryptic peptides, which were then separated using the EASY-nLC 1200 extreme performance liquid system. 90% acetonitrile and 0.1% formic acid made up solvent B. With a flow rate of 500 nL/min, the liquid gradient parameters were: 0–16 min, 6–22% solvent B; 16–22 min, 22–32% solvent B; 22–26 min, 32–80% solvent B; and 26–30 min, 80% solvent B.

Peptides were separated using ultraperformance liquid chromatography (UPLC-MS), which was followed by ionization using the NSI source and analyzed using the Q Exactive HF-X. The electrospray voltage was set to 2100 V, and the precursor and secondary fragments were identified and analyzed using a high-resolution Orbitrap. The primary MS's 400–1250 *m/z* scanning range and 120,000 scanning resolution were set. The resolution of the Secondary MS Orbitrap scan was set at 30,000. With the fragmentation energy of the HCD collision pool set at 28%, the data collection mode made use of data-independent acquisition (DIA) software. For full MS, the automatic gain control was set to 3E6, and for MS/MS, to 2E5. For both complete MS and MS/MS, the maximum implantation time (IT) was established to be 220 ms.

A search was conducted using Maxquant (v1.6.15.0) on the secondary MS data. Homo_sapiens_9606_SP_20220107.fasta (20,376 sequences) was the search database used. The mass error tolerance was adjusted at 20 ppm for fragment ions and 4.5 ppm for precursors in the First search and Main search, respectively. The minimum peptide length was set to 7, the

maximum peptide modification was set to 5, the enzyme was set to trypsin/P, and the number of missed cleavage sites was set to 2. The fixed modification was set to carbamidomethyl on Cys, while the variable modifications were set to acetylation of the protein N-terminus and oxidation on Met. Adjusted FDR was <1%.

2.3.6. Data Analysis. Skyline (v.21.2) was utilized for the processing of the generated MS data. Trypsin [KR/P] was selected as the enzyme, and 0 denoted the highest failed cleavage in the peptide parameters. The fixed alteration on Cys was carbamidomethyl, and the fixed peptide length was set at 7–25. Transition parameters: precursor charges were set to 2, 3, ion types to b, y, and ion charge to 1. The product ions were set from ion 3 to the final ion, and the ion match tolerance was set at 0.02 Da. To quantify each peptide, its fragment ion peak area was compared to the associated transitions. The statistical significance was ascertained using a two-tailed Student's *t* test, with *P* < 0.05 being the threshold for significance.

2.4. Metabolomics Analysis.
2.4.1. Sample Preparation. The frozen sample was homogenized for 20 s using a grinder set to 30 Hz after being thawed on ice. After adding an internal standard to a 400 μ L solution (methanol:water = 7:3, v/v) containing 20 mg of pulverized sample, the mixture was agitated at 1500 rpm for 5 min. The material was centrifuged at 12,000 rpm for 10 min (4 °C) after being on ice for 15 min. The supernatant was collected in a 300 μ L aliquot and kept at –20 °C for 30 min. Next, the substance was centrifuged for 3 min at 12,000 rpm (4 °C). An aliquot of 200 μ L of the supernatant was transferred for LC-MS examination.

2.4.2. High-Performance Liquid Chromatography Conditions. Every sample was collected using the LC-MS technique in compliance with its manual. The analytical conditions: Waters ACQUITY UPLC HSS T3 C18 (1.8 μ m, 2.1 mm \times 100 mm) is the column used in UPLC. The solvent system comprises acetonitrile (0.1% formic acid) and water (0.1% formic acid). The temperature is 40 °C, the flow rate is 0.4 mL/min, and the injection volume is 2 μ L. After the column was eluted with 5% mobile phase B (0.1% formic acid in acetonitrile) at 0 min, the procedures were as follows: a linear gradient to 90% mobile phase B (0.1% formic acid in acetonitrile) over 11 min, held for 1 min; and a return to 5% mobile phase B within 0.1 min, held for 1.9 min.

2.4.3. Data Processing. By application of ProteoWizard software, LC-MS converted the original data file into the mzML format. Peak extraction, peak alignment, and retention time correction were performed with the XCMS program. The “SVR” method was used to modify the peak area. Peaks with a detection rate of less than 50% were removed from each sample group. Metabolic identifying information was then discovered by searching via the metDNA, AI, integrated public databases, and self-built databases.

2.4.4. Multivariate Analysis. The R (www.r-project.org) has a statistics function called prcomp that does unsupervised principal component analysis (PCA). The unit variance was used to scale the data before they underwent unsupervised PCA. The cor function in R was utilized to calculate the Pearson correlation coefficients (PCCs) between the samples. The hierarchical cluster analysis (HCA) results of the samples and metabolites are shown alongside heatmaps. Both HCA and PCC were carried out via the R package ComplexHeatmap. The corrected signal intensities of the metabolites (unit variance scaling) for HCA are shown as a color spectrum.

2.4.5. Differential Metabolites Selection and KEGG Analysis. The variable importance for the projection (VIP) >1 and *P* value ($P < 0.05$, Student's *t* test) were adopted to identify the different metabolites for the two-group study. VIP values were generated from the orthogonal partial least-squares-discriminant analysis (OPLS-DA) results, which also contained score plots and permutation plots, using the R program MetaboAnalystR. The data were log-converted (\log_2) and mean-centered before being processed with OPLS-DA. To avoid overfitting, a 200-permutation permutation test was conducted.

After identification, metabolites were annotated by using the KEGG Compound database and linked to the KEGG Pathway database. The *P* value of a hypergeometric test indicates highly enriched pathways for a given set of metabolites.

2.5. Integrated Analysis of Proteomics and Metabolomics. We mapped the DEPs and DEMs onto the iPath overall metabolic pathway and KEGG pathway and ran KEGG enrichment analysis. After that, a correlation network was created using Spearman's correlation analysis among DEPs and DEMs with a correlation coefficient $|r| \geq 0.8$. Finally, the Metascape module of the Cytoscape program was employed to perform the interaction network visualization of the proteome and metabolome.

2.6. Statistical Analysis. SPSS 23.0 was utilized for data processing and analysis. The measurement data were expressed with average and standard deviation. A paired-sample test was applied to compare sample characteristics between the two groups. When $P < 0.05$, statistics were deemed significant.

3. RESULTS

3.1. Population Characteristics. A total of 13 patients were included in the study (5 children and 8 adults). The demographic data and diagnostic information are presented in Table 1. Five patients had a diagnosis of pressure ulcer (PU),

Table 1. Characteristics of CW Patients

case	age (year)	gender	diagnosis ^a	location
1	14	Female	PU	Sacrococcygeal
2	43	Male	PU	Sacrococcygeal
3	45	Female	PU	Sacrococcygeal
4	53	Female	PU	Sacrococcygeal
5	55	Male	PU	Occipitalia
6	1	Male	TU	Hand
7	2	Male	TU	Lower extremity
8	3	Male	TU	Upper extremity
9	5	Male	TU	Foot
10	5	Male	TU	Foot
11	16	Male	TU	Lower extremity
12	50	Male	TU	Lower extremity
13	53	Male	TU	Lower extremity

^aPU for pressure ulcer; TU for traumatic ulcer.

and eight patients were diagnosed with traumatic ulcer (TU). Among them, PU mainly occurred in the sacrococcygeal and occipital regions, while TU mostly occurred in the extremities.

3.2. Proteomics Profiles in Wound and Surrounding Tissue. **3.2.1. Protein Identification.** LC-MS/MS and label-free quantification were applied for evaluating the proteome profiles of the surrounding tissue and the wound. In the samples from the two groups, 5204 proteins were found in total, 3969 of which were quantified (Table S1). A variety of

quality control (QC) tests, including as peptide length distribution, peptide number distribution, protein coverage distribution, and protein molecular weight distribution, should be carried out following the database search to guarantee that the quality of the findings satisfies the requirements (Figures S1–S4). Finally, 82 DEPs were identified using the 1.5-fold change criterion with $P < 0.05$, including 38 upregulated and 44 downregulated proteins (Figure 2). The heatmap's color distribution indicated that the two groups' levels of protein expression differed (Figure 2C). We conducted a comprehensive bioinformatic study of proteins using these data.

3.2.2. Bioinformatic Analysis of the DEPs. GO analysis (cellular components, molecular function, and biological process) was used to categorize the DEPs (Figures S5 and S6). Among the significantly enriched keywords connected to biological components were the ECM, collagen-containing ECM, and basement membrane (Figure 3A). The biological process was significantly enhanced with respect to the ECM structure, cell motility modulation, and cell migration. Collagen binding, integrin binding, peptidase regulator activity, and cell adhesion molecule binding were shown to have substantially enriched molecular function categories (Figure 3C). Furthermore, the functional enrichment of these identified proteins was ascertained by using KEGG analysis (Figure 3D). Because of their respective relationships, we were especially interested in focal adhesion (FA) (hsa04510), ECM–receptor interaction (hsa04512), and the PI3K-Akt signaling pathway (hsa04151).

3.2.3. The PPI Network and Validation of Key DEPs. To understand the PPIs, we performed PPI analysis between the proteins included in the above three pathways and the significant DEPs (Figure 4). The network plots showed that the FBLN1, FBLN5, EFEMP1, and EFEMP2 proteins showed reciprocal relationships with those pathway-containing proteins, while the irrelevant DEPs were automatically eliminated.

Additionally, we applied PRM to validate the DEPs between the two groups. The outcomes demonstrated that there were 16 DEPs with different expression patterns, 14 of which had expression changes that were consistent with the proteome results. Similarly, the PRM validation results confirmed that FBLN1, FBLN5, and EFEMP1 were upregulated in group Z (Figure 5).

3.3. Metabolomics Profiles in Wound and Surrounding Tissue.

3.3.1. The Metabolic Profile Classification. LC-MS/MS was performed for analyzing the same samples for metabolomics research. The total number of metabolites identified (Table S2) and the results of data QC (Figures S7 and S8) are shown in the Supporting Information. Total ion chromatograms versus the QC specimens were compared in the positive (Figure 6B) and negative (Figure 6A) ion modes. The total ion currents of the metabolites had a high degree of curve overlap in the data, suggesting that the retention duration and peak intensity were both constant. This suggests that the signal stability was improved when the mass spectra were obtained for different periods of time within the same sample. The class count ring showed the species and proportion of all metabolites, with the higher proportion having benzene and substitute derivatives (18.9%), heterocyclic compounds (12.07%), and amino acids and their metabolites (10.8%) (Figure 6C).

3.3.2. Identification and Pathway Investigation of DEMs. The standards for screening of DEMs were established at $P < 0.05$, and a VIP score greater than 1. 214 DEMs were found in

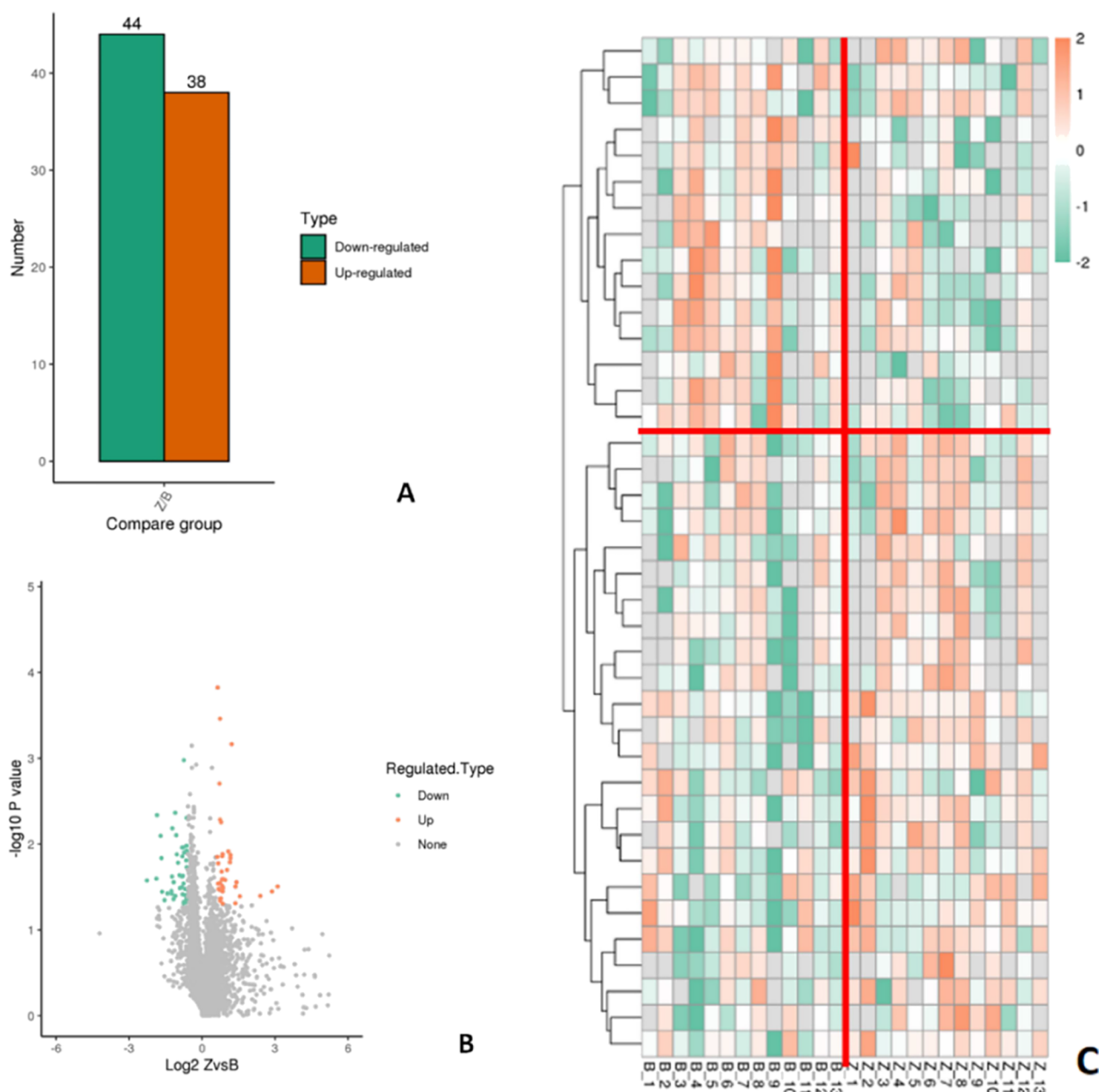


Figure 2. (A) Statistics and (B) volcano plot of DEPs between the two groups. (C) Heatmap of the intensities of DEPs between the two groups.

all, including 111 downregulated and 103 upregulated metabolites. The metabolic states of wound tissue were dramatically altered, as evidenced by the distinct separation between the two groups in the OPLS-DA score plot (Figure 7A). Heatmaps were created to illustrate the variations between the two groups in order to better comprehend the alterations (Figure 7B). These DEMs were considerably enriched in the metabolism of amino and nucleotide sugars as well as the production of nucleotide sugars according to KEGG analysis (Figure 7C).

3.4. Integrated Analysis of Proteomics and Metabolomics. To identify proteins and metabolites that differed significantly, a Spearman correlation analysis was used. Next, in order to evaluate the possible correlation between DEPs and DEMs, we analyzed the differential proteins and metabolites using the KEGG pathway analysis (Figure 8). The PI3K-Akt

signaling pathway, glycine, serine and threonine metabolism, biosynthesis of cofactors, and other processes were enhanced.

4. DISCUSSION

Treatment of CW has been challenging, and our knowledge of its associated molecular mechanisms remains sparse. We now have a better technique to investigate disease mechanisms because of the advancement of omics technology. In recent years, omics investigations of CW have revealed many novel etiologies, providing important hints for clinical diagnosis and therapy. Moreover, the local microenvironment will be greatly impacted by the protein expression and related metabolites of the wound tissue during the formation of CW. Thus, we conducted proteomics and metabolomics experiments on PU and TU to investigate molecular changes in these tissues. This is the first study that we are aware of that focuses on the tissue proteome and metabolomics related to nondiabetic CW.

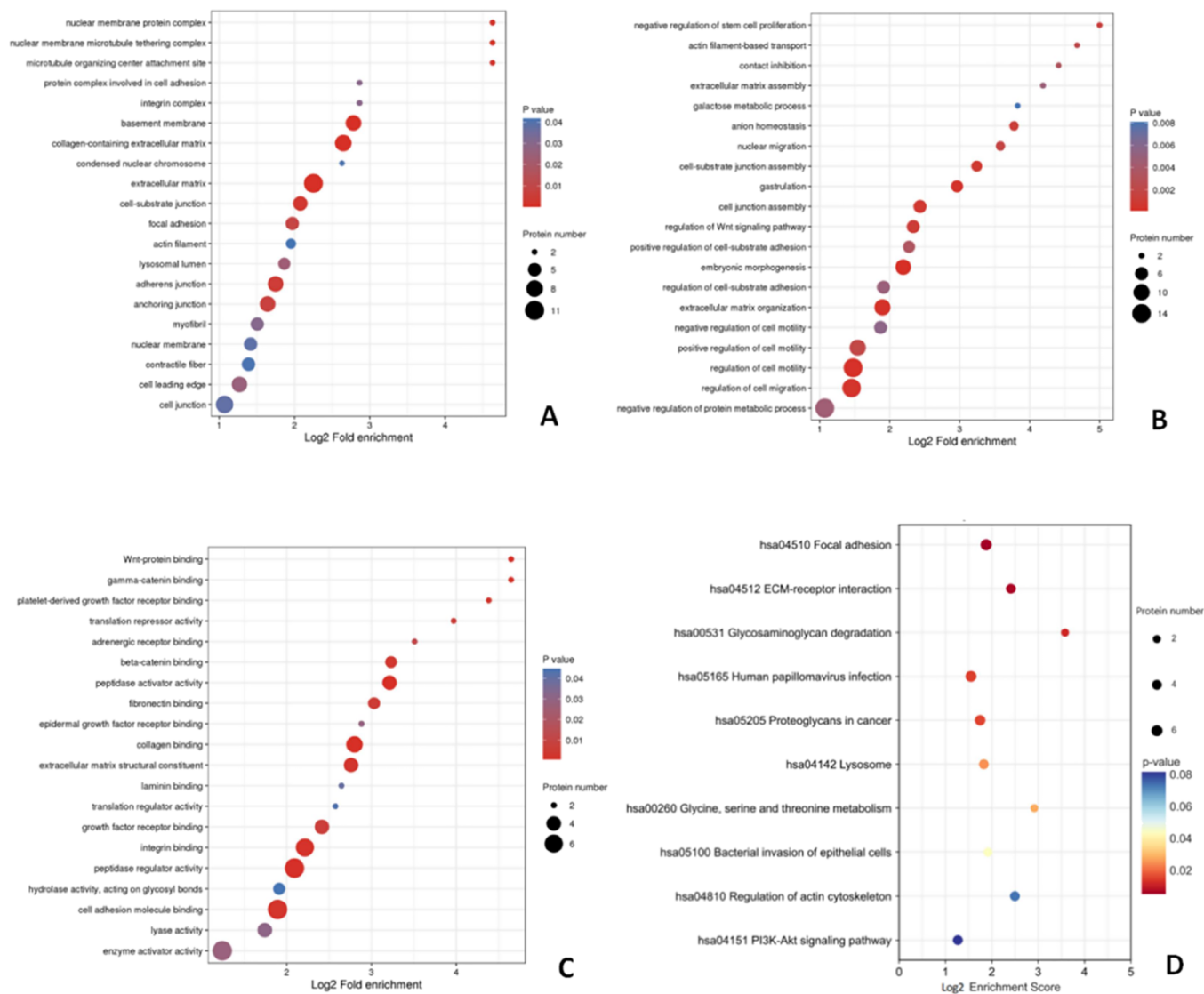


Figure 3. KEGG and GO analyses of protein differential expression. (A) Cellular component; (B) biological process; (C) molecular function; (D) KEGG pathway.

In this study, we contrasted the proteins and metabolites between the central wound and surrounding tissues and performed bioinformatics analysis. Consequently, we found 82 DEPs, 214 DEMs, and associated enriched signaling pathways and interaction networks between the two groups.

4.1. Alterations in Signaling Pathway Transduction.

According to the proteome's GO analysis, DEPs are mostly abundant in the processes that lead to ECM production, intercellular adhesion, and cell migration. Additionally, based on KEGG enrichment analysis, those DEPs mostly took a role in regulation of ECM, cell activities, and intercellular adhesion, especially FN1, IGTA2, IGTA5, and LAMA3. These proteins were implicated in a number of signaling pathways. Despite not being highly enriched, the KEGG database showed that the PI3K-Akt pathway was associated with the FA and ECM-receptor interaction pathways, and they are all involved in the same transduction process¹⁷ (Figure S7). These pathways influence cellular activities and signaling processes and may be directly connected to the development of the CW.

FA, which is important for cell mobility, proliferation, differentiation, gene expression control, and cell survival,

mediates the attachment of cells to the ECM. A multimolecular complex of FA proteins in FA anchors actin filaments to integrin family transmembrane receptors. The critical kinase in this pathway is focal adhesion kinase (FAK), which mediates several signaling pathways and is crucial for cell signal transduction. FAK may activate intracellular signaling pathways, including PI3K/Akt and Ras/MAPK, and integrate signals from integrins, growth factors, and mechanical stimuli. The actin cytoskeleton recombines as a result of these signaling events, and this process is necessary for modifications to a cell's movements, structure, and genetic expression.^{18,19}

The ECM is a complex combination that is fundamental to tissue and organ formation as well as cell and tissue structure and function. The ECM-receptor interaction pathway is responsible for signal transmission and particular cell-ECM interactions. Transmembrane molecules, mainly integrins, mediate this process. Integrins are cell adhesion molecules that link the cytoskeleton to the ECM. Integrins, as tissue cytoskeleton adhesion receptors, play a key role in signaling pathways that regulate a number of events, such as proliferation, differentiation, apoptosis, and cell migration.^{20,21}

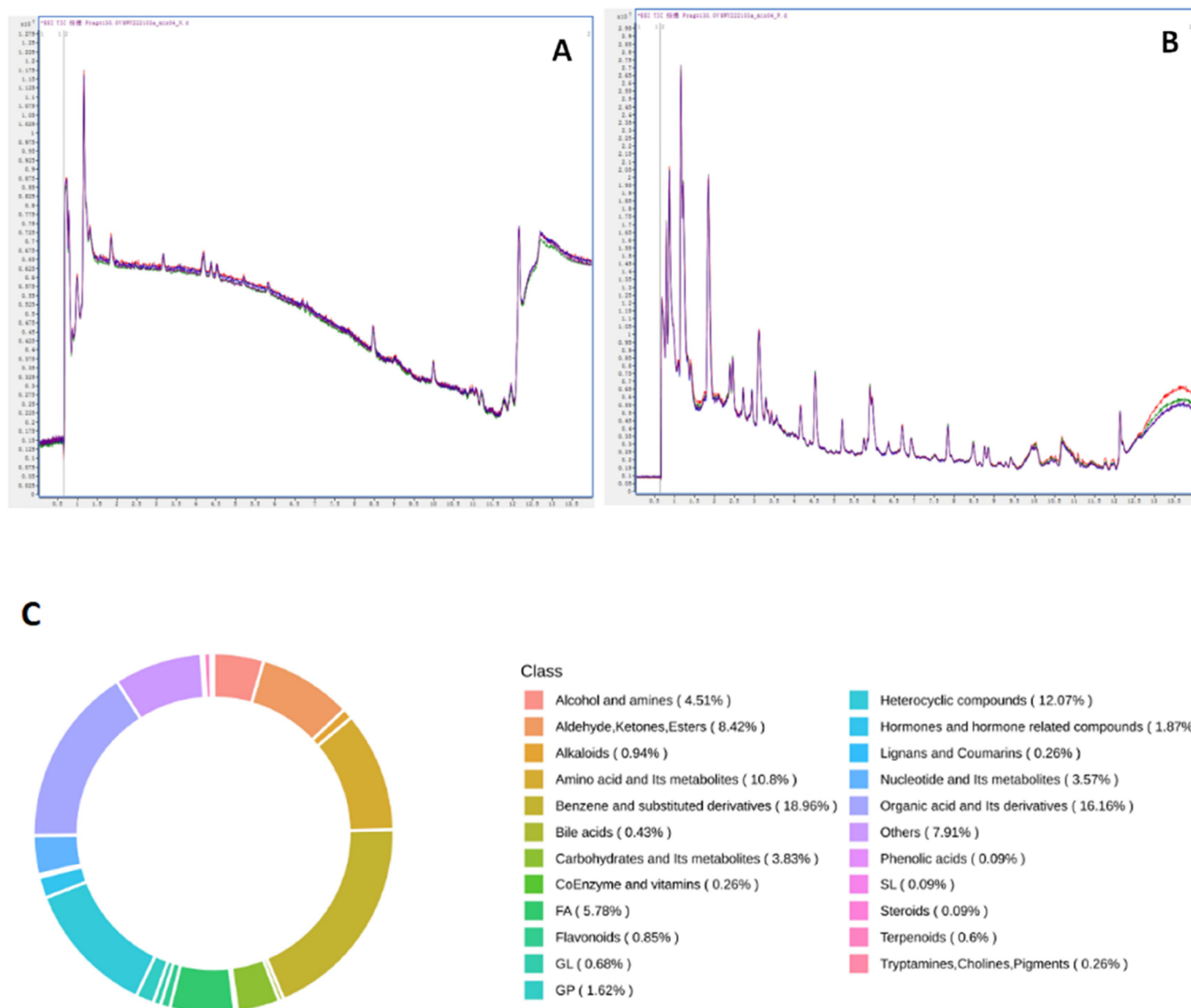


Figure 6. Chromatographs with typical base peak intensities: (A) negative and (B) positive ion modes; (C) class count ring of all metabolites.

Interestingly, we found some signaling pathways that were jointly enriched by DEPs and DEMs in the correlation analysis. Due to the altered expression of certain proteins and metabolites, these pathways may be more intimately associated with the development of CW. Remarkably, we observed several modifications in a classical signal transduction pathway.

The PI3K/Akt/mTOR pathway serves as an important signaling route in mammalian cells.²³ It suppresses apoptosis and promotes cell growth by influencing the activation state of several downstream effector molecules. We noticed that in the tissue samples of group Z, which was implicated in the cAMP signaling pathway. Succinic acid and AMP quantities were reduced, and protein PAK1 expression was downregulated by combining the findings of correlation analysis and KEGG database information. These anomalies influence not only vascular endothelial cell cytoskeletal reorganization and adherent junction enhancement but also the downstream PI3K-Akt pathway.

As mentioned above, this pathway controls essential cellular functions, and FA and ECM–receptor interaction pathways are involved in its initial stages. The FN1 and IGTAS proteins,

which participate in these two pathways, were upregulated in group Z samples along with LAMA3 and decreased IGTA2 protein expression according to differential analysis. Additionally, AMP expression was reduced, and these changes may have influenced the downstream AMPK signaling pathway during transduction, resulting in an increase in FASN expression and glucose levels, which were the differences in proteins and metabolites that we observed in group Z.

Although we did not find extra downstream signaling pathways that were highly enriched, the changes in transduction may still have an effect on the downstream mTOR signaling pathway (Figure 9), which is essential for glycerolipid metabolism, autophagy control, and protein synthesis.²⁴ Collectively, our results support the idea that changes in this group of signaling mechanisms may contribute to CW formation.

4.3. Potential Biomarkers of CW. Among the 82 DEPs between the two groups, 44 proteins were downregulated and 38 proteins were upregulated, which were also the source of our screening for potential biomarkers. Candidate biomarkers could be initially determined via bioinformatics and data from

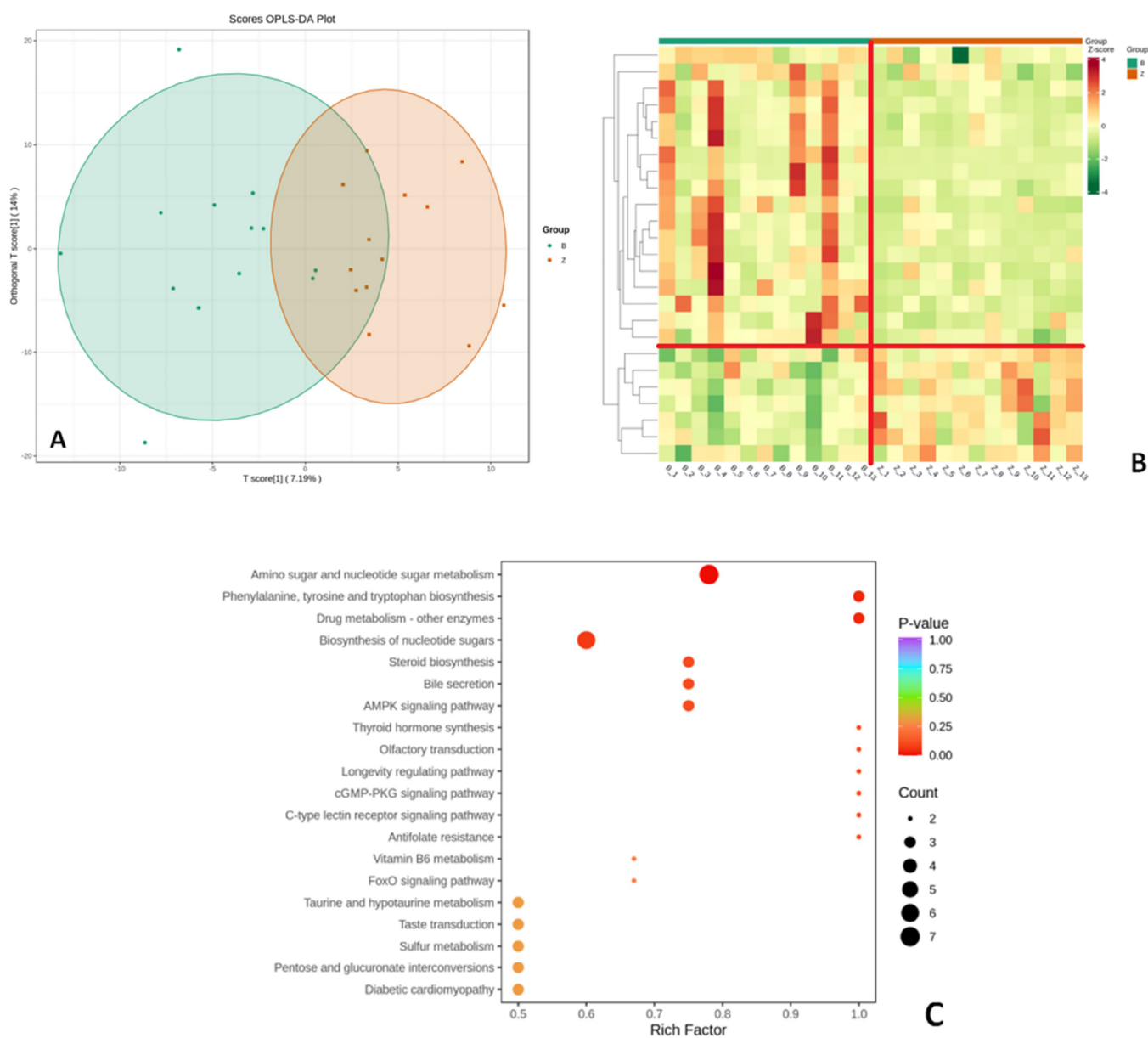


Figure 7. (A) The OPLS-DA score map with QC sample; (B) Heatmap of the intensities of differentially abundant metabolites between the two groups. (C) Bubble chart of differentially abundant metabolites and corresponding enriched pathways.

open databases. To determine relationships among DEPs with significant differences, we performed an interaction analysis. The network created by PPI demonstrates that FA, ECM receptor interaction, and the PI3K-Akt signaling pathway are linked to most DEPs. For FBLN1, FBLN5, EFEMP1, and EFEMP2, however, no relevant pathway information was available, although they were only associated with the above signaling pathways. Subsequently, through PRM verification, we further confirmed that the expression differences of FBLN1, FBLN5, and EFEMP1 in the two groups of samples did exist.

The UniProt database (<https://www.uniprot.org/>) indicates that FBLN1 (Fibulin-1) is a matrix fiber that contains fibronectin (FN). FBLN1 dramatically decreased cell adherence and migration in the ECM. Additionally, cells over-expressing FBLN1 had decreased motility in terms of speed, range, and duration. However, not all cell types exhibit this characteristic. Finally, the study discovered that FBLN1 may

influence cell adhesion and movement by controlling the actin–myosin motor complex signal transduction pathway.²⁵

The ECM protein FBLN5 (fibulin-5) is crucial for angiogenesis, plays a role in vascular remodeling, and regulates the adhesion, mobility, and proliferation of endothelial cells. Additionally, FBLN5 participates in continuous elastin (ELN) polymer formation, promoting interactions between micro-fibers and ELNs that are critical to the structural and functional integrity of a range of tissues, including blood vessels, the lungs, skin, and bone.^{26,27} However, increased FBLN5 expression also inhibited cellular activity. According to research by Furie et al.²⁸ on the effects of FBLN5 on the adhesion and proliferation of keloid fibroblasts, the proliferation rate of keloid fibroblasts coated with FBLN5 was significantly lower, and adhesion was delayed. Furthermore, for tumor cells, FBLN5 reduced the adherence and migration of hepatocellular carcinoma cells to FN in a concentration-dependent manner. Additionally, downregulating MMP-7 prevented tumor cell

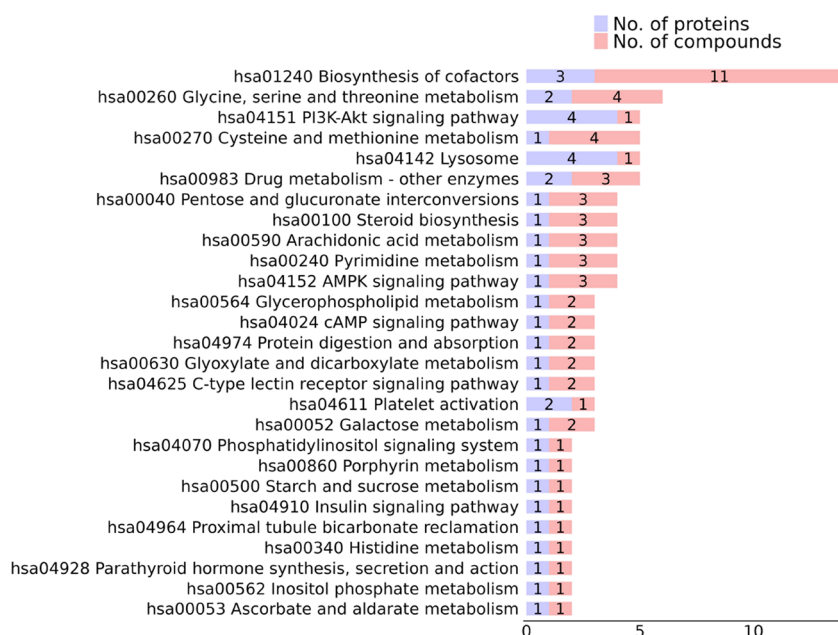


Figure 8. KEGG pathway inscription of DEPs and DEMs.

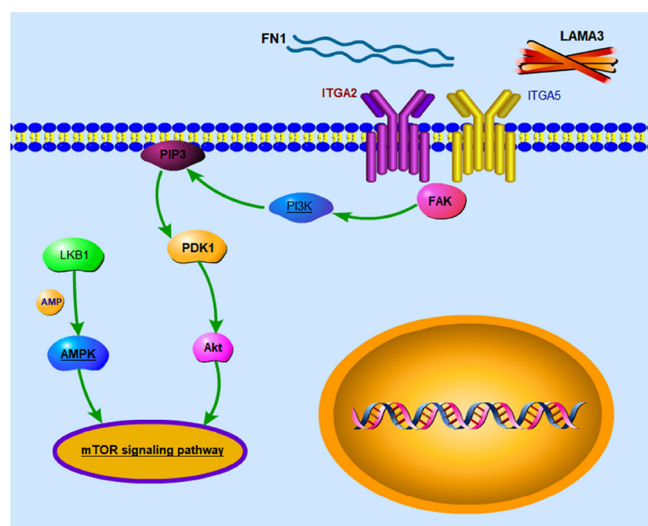


Figure 9. Part of the PI3K/Akt/mTOR signal transduction pathways.

motility and invasion via an integrin-binding arginine–glycine–aspartic acid motif.²⁹ Later, Chan et al.³⁰ reported that FBLN5 can tightly attach to the surface of vascular endothelial cells and exert potent antiangiogenic effects by impairing the Ang-1/TIE-2 receptor axis signaling pathway and decreasing the vitality of endothelial cells. This finding further sheds light on the mechanism by which FBLN5 affects the cell function.

The EFEMP1, also known as FBLN3, is an epithelial growth factor (EGF)-containing fibulin-like ECM protein, which is homologous to FBLN5 and expressed in endothelial cells. Albig et al.³¹ found that constitutively expressed FBLN-3 suppresses angiogenic sprouting, invasion, and proliferation of endothelial cells and is altered in a number of human malignancies. In addition, the central nervous system tumor cells had expressed FBLN3, which would result in higher expression of matrix metalloproteinases, which leads to the

excessive degradation of ECM and assists in tumor cell invasion.³²

Another study reported that the FBLN3 can compete with EGF in pancreatic cancer cells and bind to the EGF receptor (EGFR), which activates downstream signaling pathways and causes EGFR autophosphorylation.³³ Together, FBLN1, 3, and 5 were essential for cellular functions. The skin and blood vessel cells will be negatively affected by their higher expression levels in tissues, and the ECM may be an accomplice in the development of CW. The outcomes we achieved in the present study are consistent with the facts stated above.

However, there are several limitations to be noted in the current research. There was a rather small sample size. CW is a complex trait resulting from pathogenesis, individual differences, and the wound microenvironment factors. The main limitations that restrict the generalizability of the results we obtained are age, gender, and type of CW. In the absence of mechanistic research, it is unclear how DEPs and DEM affect wound healing through related signaling pathways. Hence, we will focus on this part in future studies to verify the current results.

5. CONCLUSIONS

According to the findings of this study, the upstream and downstream signaling pathways of the PI3K-Akt pathway are associated with the development of CW. Furthermore, compared to the wound's surrounding tissue, the expression of FBLN1, 3, and 5 proteins in the wound's central tissue was significantly increased, inhibiting the proliferation and function of skin and vessel-related cells and resulting in extended wound healing. However, as this study is exploratory, it is quite difficult to fully understand the intricacy of our results. To find causative variations, confirmatory mechanistic research *in vitro* and *in vivo* is necessary.

ASSOCIATED CONTENT

Supporting Information

The Supporting Information is available free of charge at <https://pubs.acs.org/doi/10.1021/acsomega.4c01335>.

Overview of protein identification between two groups and data quality control results, GO analysis, and COG/KOG functional classification map of differentially expressed proteins, total number of identified metabolites and data quality control results, diagram of PI3K-Akt, and its downstream signal transduction pathways (PDF)

AUTHOR INFORMATION

Corresponding Authors

Zhu Xiong – Department of Orthopedics, Shenzhen Children's Hospital, Shenzhen, Guangdong 518026, P. R. China; Email: bamboobear@163.com

Lei Yang – Department of Burns, Nanfang Hospital, Southern Medical University, Guangzhou, Guangdong 510515, P. R. China; Email: yuanyang@smu.edu.cn

Authors

Shuaidan Zeng – Department of Burns, Nanfang Hospital, Southern Medical University, Guangzhou, Guangdong 510515, P. R. China; Department of Orthopedics, Shenzhen Children's Hospital, Shenzhen, Guangdong 518026, P. R. China; orcid.org/0000-0002-9003-2721

Zijun Zheng – Department of Burns, Nanfang Hospital, Southern Medical University, Guangzhou, Guangdong 510515, P. R. China

Xuerong Wei – Department of Burns, Nanfang Hospital, Southern Medical University, Guangzhou, Guangdong 510515, P. R. China

Lianglong Chen – Department of Burns, Nanfang Hospital, Southern Medical University, Guangzhou, Guangdong 510515, P. R. China

Jiabao Lin – Department of Burns, Nanfang Hospital, Southern Medical University, Guangzhou, Guangdong 510515, P. R. China

Mengqian Liu – Department of Burns, Nanfang Hospital, Southern Medical University, Guangzhou, Guangdong 510515, P. R. China

Kaize Zheng – Department of Orthopedics, Shenzhen Children's Hospital, Shenzhen, Guangdong 518026, P. R. China

Weiqing Li – Department of Orthopedics, Shenzhen Children's Hospital, Shenzhen, Guangdong 518026, P. R. China

Xiaodi Chen – Department of Orthopedics, Shenzhen Children's Hospital, Shenzhen, Guangdong 518026, P. R. China

Jun Ma – Department of Burns, Nanfang Hospital, Southern Medical University, Guangzhou, Guangdong 510515, P. R. China

Complete contact information is available at:

<https://pubs.acs.org/10.1021/acsomega.4c01335>

Funding

This work was supported by the National Natural Science Foundation of China [No. 82372526], Guangdong Basic and Applied Basic Research Foundation [No. 2023A1515012970], and Sanming Project of Medicine in Shenzhen of China [SZSM202011012].

Notes

The authors declare no competing financial interest.

ACKNOWLEDGMENTS

We thank Jingjie PTM BioLab (Hangzhou) Co, Ltd in China for the omics analysis. We also thank Teng Li and Taifeng Jiang for providing technical support and assistance in the analysis of the results.

REFERENCES

- (1) Graves, N.; Phillips, C. J.; Harding, K. A narrative review of the epidemiology and economics of chronic wounds. *Br J. Dermatol.* **2022**, *187* (2), 141–148.
- (2) Jones, R. E.; Foster, D. S.; Longaker, M. T. Management of Chronic Wounds-2018. *JAMA* **2018**, *320* (14), 1481–1482.
- (3) Frykberg, R. G.; Banks, J. Challenges in the treatment of chronic wounds. *Adv. Wound Care (New Rochelle)* **2015**, *4*, 560–582.
- (4) Ramirez, H. A.; Liang, L.; Pastar, I.; et al. Comparative Genomic, MicroRNA, and Tissue Analyses Reveal Subtle Differences between Non-Diabetic and Diabetic Foot Skin. *PLoS One* **2015**, *10* (8), No. e0137133.
- (5) Icli, B.; Wu, W.; Ozdemir, D.; et al. MicroRNA-135a-3p regulates angiogenesis and tissue repair by targeting p38 signaling in endothelial cells. *FASEB J.* **2019**, *33* (4), 5599–5614.
- (6) Zhong, H.; Qian, J.; Xiao, Z.; Chen, Y.; He, X.; Sun, C.; Zhao, Z.; Durazzo, A.; et al. MicroRNA-133b Inhibition Restores EGFR Expression and Accelerates Diabetes-Impaired Wound Healing. *Oxid Med. Cell. Longev.* **2021**, *2021* (27), No. 9306760.
- (7) Janusz, M.; Chen, K.; Henn, D.; et al. Characterization of Diabetic and Non-Diabetic Foot Ulcers Using Single-Cell RNA-Sequencing. *Micromachines (Basel)* **2020**, *11* (9), 815.
- (8) Theodoridis, G.; Baltzis, D.; Roustis, M.; et al. Integrated Skin Transcriptomics and Serum Multiplex Assays Reveal Novel Mechanisms of Wound Healing in Diabetic Foot Ulcers. *Diabetes* **2020**, *69* (10), 2157–2169.
- (9) Stolzenburg-Veesser, L.; Golubnitschaja, O. Mini-encyclopaedia of the wound healing -Opportunities for integrating multi-omic approaches into medical practice. *J. Proteomics* **2018**, *188*, 71–84.
- (10) Kim, J.; Yang, G. S.; Lyon, D.; et al. Metabolomics: Impact of Comorbidities and Inflammation on Sickness Behaviors for Individuals with Chronic Wounds. *Adv. Wound Care (New Rochelle)* **2021**, *10* (7), 357–369.
- (11) Álvarez-Rodríguez, I. I.; Castaño-Tostado, E.; García-Gutiérrez, D. G.; Reynoso-Camacho, R.; Elton-Puente, J. E.; Barajas-Pozos, A.; Pérez-Ramírez, I. F.; et al. Non-Targeted Metabolomic Analysis Reveals Serum Phospholipid Alterations in Patients with Early Stages of Diabetic Foot Ulcer. *Biomark. Insights* **2020**, *15*, No. 1177271920954828.
- (12) Bandyk, D. F. The diabetic foot: Pathophysiology, evaluation, and treatment. *Semin Vasc Surg* **2018**, *31* (2–4), 43–48.
- (13) Soyoye, D. O.; Abiodun, O. O.; Ikem, R. T.; et al. Diabetes and peripheral artery disease: A review. *World J. Diabetes* **2021**, *12* (6), 827–838.
- (14) Kwek, M. S. Y.; Thangaveloo, M.; Hui, S. L. B.; et al. Characterisation of an ischemia-reperfusion model for the formation of a stage I pressure ulcer in mouse skin. *J. Tissue Viability* **2021**, *30* (3), 352–362.
- (15) Olivier, M.; Asmis, R.; Hawkins, G. A.; et al. The Need for Multi-Omics Biomarker Signatures in Precision Medicine. *Int. J. Mol. Sci.* **2019**, *20*, 4781.
- (16) Lu, M.; Zhan, X. The crucial role of multiomic approach in cancer research and clinically relevant outcomes. *EPMA J.* **2018**, *9*, 77–102.
- (17) <https://www.kegg.jp/entry/map04510>.
- (18) Petit, V.; Thiery, J. P. Focal adhesions: structure and dynamics. *Biol. Cell.* **2000**, *92* (7), 477–494.
- (19) Mitra, S. K.; Hanson, D. A.; Schlaepfer, D. D. Focal adhesion kinase: in command and control of cell motility. *Nat. Rev. Mol. Cell Biol.* **2005**, *6* (1), 56–68.

- (20) Bosman, F. T.; Stamenkovic, I. Functional structure and composition of the extracellular matrix. *J. Pathol.* **2003**, *200* (4), 423–428.
- (21) van der Flier, A.; Sonnenberg, A. Function and interactions of integrins. *Cell Tissue Res.* **2001**, *305* (3), 285–298.
- (22) Osaki, M.; Oshimura, M.; Ito, H. PI3K-Akt pathway: its functions and alterations in human cancer. *Apoptosis.* **2004**, *9* (6), 667–676.
- (23) Ersahin, T.; Tuncbag, N.; Cetin-Atalay, R. The PI3K/AKT/mTOR interactive pathway. *Mol. Biosyst.* **2015**, *11* (7), 1946–1954.
- (24) Glaviano, A.; Foo, A. S. C.; Lam, H. Y.; Yap, K. C. H.; Jacot, W.; Jones, R. H.; Eng, H.; Nair, M. G.; Makvandi, P.; Georger, B.; Kulke, M. H.; Baird, R. D.; Prabhu, J. S.; Carbone, D.; Pecoraro, C.; Teh, D. B. L.; Sethi, G.; Cavalieri, V.; Lin, K. H.; Javidi-Sharifi, N. R.; Toska, E.; Davids, M. S.; Brown, J. R.; Diana, P.; Stebbing, J.; Fruman, D. A.; Kumar, A. P. PI3K/AKT/mTOR signaling transduction pathway and targeted therapies in cancer. *Mol. Cancer.* **2023**, *22* (1), 138.
- (25) Twal, W. O.; Czirok, A.; Hegedus, B.; Knaak, C.; Chintalapudi, M. R.; Okagawa, H.; Sugi, Y.; Argraves, W. S. Fibulin-1 suppression of fibronectin-regulated cell adhesion and motility. *J. Cell Sci.* **2001**, *114* (24), 4587–4598.
- (26) El-Hallous, E.; Sasaki, T.; Hubmacher, D.; Getie, M.; Tiedemann, K.; Brinckmann, J.; Bätge, B.; Davis, E. C.; Reinhardt, D. P. Fibrillin-1 interactions with fibulins depend on the first hybrid domain and provide an adaptor function to tropoelastin. *J. Biol. Chem.* **2007**, *282* (12), 8935–8946.
- (27) Guadall, A.; Orriols, M.; Rodríguez-Calvo, R.; Calvayrac, O.; Crespo, J.; Aledo, R.; Martínez-González, J.; Rodríguez, C. Fibulin-5 is up-regulated by hypoxia in endothelial cells through a hypoxia-inducible factor-1 (HIF-1 α)-dependent mechanism. *J. Biol. Chem.* **2011**, *286* (9), 7093–7103.
- (28) Furie, N.; Shteynberg, D.; Elkhatib, R.; Perry, L.; Ullmann, Y.; Feferman, Y.; Preis, M.; Flugelman, M. Y.; Tzchori, I. Fibulin-5 regulates keloid-derived fibroblast-like cells through integrin beta-1. *Int. J. Cosmet. Sci.* **2016**, *38* (1), 35–40.
- (29) Tang, J. C.; Liu, J. H.; Liu, X. L.; Liang, X.; Cai, X. J. Effect of fibulin-5 on adhesion, migration and invasion of hepatocellular carcinoma cells via an integrin-dependent mechanism. *World J. Gastroenterol.* **2015**, *21* (39), 11127–11140.
- (30) Chan, W.; Ismail, H.; Mayaki, D.; Sanchez, V.; Tiedemann, K.; Davis, E. C.; Hussain, S. N. Fibulin-5 Regulates Angiopoietin-1/Tie-2 Receptor Signaling in Endothelial Cells. *PLoS One.* **2016**, *11* (6), No. e0156994.
- (31) Albig, A. R.; Neil, J. R.; Schiemann, W. P. Fibulins 3 and 5 antagonize tumor angiogenesis *in vivo*. *Cancer Res.* **2006**, *66* (5), 2621–2629.
- (32) Hu, B.; Thirtamara-Rajamani, K. K.; Sim, H.; Viapiano, M. S. Fibulin-3 is uniquely upregulated in malignant gliomas and promotes tumor cell motility and invasion. *Mol. Cancer Res.* **2009**, *7* (11), 1756–1770.
- (33) Camaj, P.; Seeliger, H.; Ischenko, I.; Krebs, S.; Blum, H.; De Toni, E. N.; Faktorova, D.; Jauch, K. W.; Bruns, C. J. EFEMP1 binds the EGF receptor and activates MAPK and Akt pathways in pancreatic carcinoma cells. *Biol. Chem.* **2009**, *390* (12), 1293–1302.